Article

Quijarroite, $Cu_6HgPb_2Bi_4Se_{12}$, a New Selenide from the El Dragón Mine, Bolivia

Hans-Jürgen Förster [1],*, Luca Bindi [2], Günter Grundmann [3] and Chris J. Stanley [4]

[1]   Helmholtz Centre Potsdam German Research Centre for Geosciences GFZ, DE-14473 Potsdam, Germany
[2]   Dipartimento di Scienze della Terra, Università degli Studi di Firenze, Via G. La Pira 4, I-50121 Firenze, Italy; luca.bindi@unifi.it
[3]   Eschenweg 6, DE-32760 Detmold, Germany; grundmann.g@gmx.de
[4]   Department of Earth Sciences, Natural History Museum, Cromwell Road, London SW7 5BD, UK; c.stanley@nhm.ac.uk
*   Correspondence: hans-juergen.foerster@gfz-potsdam.de; Tel.: +49-0331-288-28843

Abstract: Quijarroite, ideally $Cu_6HgPb_2Bi_4Se_{12}$, is a new selenide species from the El Dragón mine, Department of Potosí, Bolivia. It most frequently occurs as lath-shaped thin plates (up to 150 μm in length and 20 μm in width) intimately (subparallel) intergrown with hansblockite, forming an angular network-like intersertal texture. Quijarroite is occasionally also present as sub- to anhedral grains up to 200 μm in length and 50 μm in width. It is non-fluorescent, black and opaque with a metallic luster and black streak. It is brittle, with an irregular fracture and no obvious cleavage and parting. In plane-polarized incident light, quijarroite is weakly pleochroic from cream to very slightly more brownish-cream, displaying no internal reflections. Between crossed polars, quijarroite is moderately anisotropic with pale orange-brown to blue rotation tints. Lamellar twinning on {110} is common; parquet twinning occurs rarely. The reflectance values in the air for the COM (Commission on Ore Mineralogy) standard wavelengths (R_1 and R_2) are: 46.7, 46.8 (470 nm), 47.4, 48.2 (546 nm), 47.1, 48.5 (589 nm), and 46.6, 48.7 (650 nm). Electron-microprobe analyses yielded a mean composition of Cu 13.34, Ag 1.02, Hg 7.67, Pb 16.87, Co 0.03, Ni 0.15, Bi 27.65, Se 33.52, total 100.24 wt %. The mean empirical formula, normalized to 25 *apfu* (atoms per formula unit), is $(Cu_{5.84}Ag_{0.26})_{\Sigma = 6.10}(Hg_{1.06}Ni_{0.07}Co_{0.01})_{\Sigma = 1.14}Pb_{2.27}Bi_{3.68}Se_{11.81}$ ($n = 24$). The simplified formula is $Cu_6HgPb_2Bi_4Se_{12}$. Quijarroite is orthorhombic, space group $Pmn2_1$, with $a = 9.2413(8)$, $b = 9.0206(7)$, $c = 9.6219(8)$ Å, $V = 802.1(1)$ Å^3, $Z = 1$. The calculated density is 5.771 g·cm^{-3}. The five strongest X-ray powder-diffraction lines (d in Å (I/I_0) (hkl)) are: 5.36 (55) (111), 3.785 (60) (211), 3.291 (90) (022), 3.125 (100) (212), and 2.312 (50) (400). The crystal structure of quijarroite can be considered a galena derivative and could be derived from that of bournonite. It is a primary mineral, deposited from an oxidizing low-T hydrothermal fluid at a f_{Se_2}/f_{S_2} ratio greater than unity. The new species has been approved by the IMA-CNMNC (2016-052) and is named for the Quijarro Province in Bolivia, in which the El Dragón mine is located.

Keywords: quijarroite; copper; bismuth; lead; mercury; selenium; bournonite structure; El Dragón; Bolivia

1. Introduction

The Andes of Bolivia host two selenide occurrences of mineralogical interest: Pacajake, District of Hiaco de Charcas, and El Dragón, Province of Antonio Quijarro, both in the Department of Potosí. The geology and ore mineralization of the El Dragón mine was first explored by Grundmann et al. (1990) [1]. It is the type locality of eldragónite, $Cu_6BiSe_4(Se_2)$ [2]; favreauite,

$PbBiCu_6O_4(SeO_3)_4(OH)\cdot H_2O$ [3]; grundmannite, $CuBiSe_2$ [4]; hansblockite, $(Cu,Hg)(Bi,Pb)Se_2$ [5]; and alfredopetrovite, $Al_2(Se^{4+}O_3)_3\cdot 6H_2O$ [6]. This Se mineralization also contains the recently discovered orthorhombic modification of $CuSe_2$, petříčekite, as a late-stage phase [7].

This paper provides the description of a new species in the Cu−Hg−Pb−Bi−Se system, quijarroite, ideally $Cu_6HgPb_2Bi_4Se_{12}$, from El Dragón. The most frequently associated minerals include hansblockite, unnamed phase "C" [4], empirical formula $Cu_4HgPb_2Bi_4Se_{11}$ (normalized to 22 atoms per formula unit, *apfu*), clausthalite, PbSe, and watkinsonite, $Cu_2PbBi_4Se_8$.

The new species quijarroite and its name have been approved by the Commission on New Minerals, Nomenclature and Classification (CNMNC) of the IMA, proposal 2016-052. The holotype specimen, representing the X-rayed crystal, is deposited in the Florence Museum, catalogue number 3232/I. The polished section, from which the holotype crystal fragment was extracted, is housed in the collections of the Natural History Museum, London, catalogue number BM 2016, 26. The cotype material, consisting of a quijarroite-bearing section, is deposited within the Mineralogical State Collection Munich (Mineralogische Staatssammlung München, Museum "Reich der Kristalle"), inventory number MSM 73573.

The name is for the Quijarro Province in Bolivia, in which the El Dragón mine is located. Quijarro also hosts the world-known Porco Ag−Zn−Pb−Sn deposit, which has been in operation since the 1500s [8].

2. Geology

The El Dragón selenide occurrence is situated in southwestern Bolivia, in the Cordillera Oriental, some 30 km southwest of Cerro Rico de Potosí. The abandoned mine is located 19°49′23.90′′ S (latitude), 65°55′00.60′′ W (longitude), at an altitude of 4160 m above sea level. The adit of the El Dragón mine is on the orographic left side of the Rio Jaya Mayu, cutting through a series of thinly stratified, pyrite-rich black shales and reddish-grey, hematite-bearing siltstones of probably Devonian age, dipping 40° to the north. The almost-vertical ore vein is located in the center of a 1.5-m-wide shear zone (average trend 135 degrees). In 1988, the selenium mineralization consisted of a single vein of small longitudinal extension (maximum 15-m-long gallery), ranging mostly from 0.5 to 2 cm in thickness.

The El Dragón mineralization represents a multi-phase assemblage of primary and secondary minerals, among which Se-bearing phases are the most prominent [1,2]. The full list of minerals recorded from El Dragón is given on [9]. A comprehensive survey of the mineralogy and origin of the El Dragón mineralization forms the subject of a companion study [10], in this issue.

3. Physical and Optical Properties

Quijarroite most frequently occurs as lath-shaped thin plates (up to 150 μm in length and 20 μm in width) intimately (subparallel) intergrown with hansblockite and, rarely, unnamed phase "C" [4], forming an angular network-like intersertal texture (Figure 1). Phase "C" occurs in the interstices of the quijarroite/hansblockite intersertal intergrowths, often together with Co-rich penroseite, $NiSe_2$, umangite, Cu_3Se_2, klockmannite, CuSe, watkinsonite, and clausthalite.

More rarely, quijarroite also forms sub- to anhedral grains up to 200 μm in length and 50 μm in width, occurring either alone in the matrix or intergrown with watkinsonite, clausthalite, eldragónite, krut'aite-penroseite, $CuSe_2$-$NiSe_2$, eskebornite, $CuFeSe_2$, klockmannite and umangite (Figures 2 and 3). Minerals occasionally being in grain-boundary contact encompass petrovicite, $Cu_3HgPbBiSe_5$, grundmannite, and native gold.
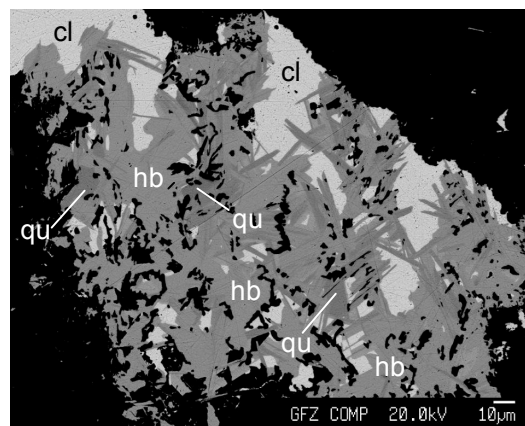
Figure 1. Back-scattered electron (BSE) image showing quijarroite (qu, dark grey) subparallel to and intergrown with hansblockite (hb, light grey) and associated with clausthalite (cl, bright).
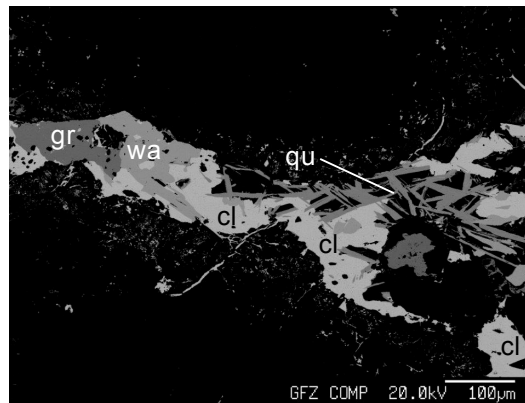
Figure 2. BSE image showing acicular grains of quijarroite (qu) in the matrix and intergrown with watkinsonite (wa) and clausthalite (cl), and associated with grundmannite (gr).

Figure 3. Reflected light digital images of quijarroite (qu) in association with hansblockite (hb), clausthalite (cl), krut'aite-penroseite (k-p), klockmannite (kl), umangite (u), and eldragónite (eld). Horizontal field of view is 200 μm. Left images: one polarizer; right images: Partly crossed polarizers.

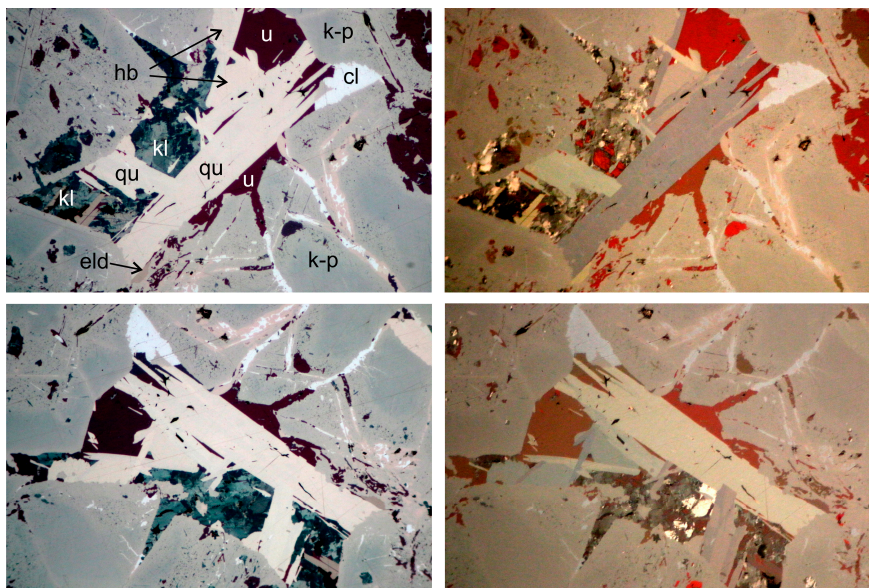Quijarroite is black in color. The mineral is opaque in transmitted light and exhibits a metallic luster. No cleavage and parting is observed and the fracture is irregular. The density and Mohs hardness could not be measured owing to the small fragment size. The calculated density (for $Z = 1$) for the empirical formula (see below) and unit-cell parameters derived from X-ray single-crystal measurements is 5.771 g/cm^3.

In plane-polarized incident light, quijarroite is weakly pleochroic from cream to very slightly more brownish-cream. The mineral does not show any internal reflections. Between crossed polars, quijarroite is moderately anisotropic with pale orange-brown to blue rotation tints (cf. Figure 3). Lamellar twinning on {110} is common; parquet twinning occurs rarely. Quantitative reflectance measurements were performed in air relative to a WTiC standard by means of a J & M TIDAS diode array spectrometer (J & M Analytik AG, Essingen, Germany) using ONYX software on a Zeiss Axioplan ore microscope (Carl Zeiss AG, Oberkochen, Germany) (Table 1). Measurements were made on unoriented grains at extinction positions, leading to the designation of R_1 (minimum) and R_2 (maximum).

Table 1. Reflectance data for quijarroite.

λ (nm)	R_1 (%)	R_2 (%)	λ (nm)	R_1 (%)	R_2 (%)
400	45.1	45.6	560	47.30	48.4
420	45.3	45.8	580	47.2	48.5
440	45.7	46.1	600	47.0	48.6
460	46.4	46.6	620	46.8	48.7
480	46.9	47.0	640	46.6	48.7
500	47.3	47.5	660	46.5	48.7
520	47.7	47.8	680	46.4	48.7
540	47.4	48.1	700	46.3	48.8

Reflectance percentages for the four COM (Commission on Ore Mineralogy) wavelengths (R_1 and R_2) are: 46.7, 46.8 (470 nm); 47.4, 48.2 (546 nm); 47.1, 48.5 (589 nm); 46.6, 48.7 (650 nm).

4. Chemical Data

Quijarroite was checked for concentrations of Cu, Ag, Pb, Hg, Fe, Co, Ni, As, Sb, Bi, S and Se. Quantitative chemical analyses were conducted in wavelength-dispersive (WDS) mode, using a JEOL thermal field-emission-type electron probe X-ray microanalyzer (FE-EPMA) JXA-8500F (JEOL Ltd., Akishima, Japan). The probe was operated at 20 kV, 20 nA; the beam size was 1–2 μm. The counting time on the peak was 20 s, with half that time on the background on both sites of the peak. The following standards, emission lines and analyzing crystals (in parentheses) were used: Cu—synthetic Cu-metal, *K*α (LIF); Ag—naumannite, *L*α (PETJ); Pb—clausthalite, *M*α (PETH); Hg—cinnabar, *L*α (LIF); Fe—pyrite, *K*α (LIF); Co—skutterudite, *K*α (LIF); Ni—pentlandite, *K*α (LIF); As—skutterudite, *L*α (TAP); Sb—stibnite, *L*α (PETJ); Bi—synthetic Bi_2Se_3, *M*α (PETH); S—sphalerite, *K*α (PETJ); Se—naumannite, *K*α (LIF). The CITZAF routine in the JEOL software, which is based on the Φ(ρZ) method [11], was used for data processing. The composition of the grain used for the structural study corresponds chemically to the other grains analyzed by the microprobe. All grains are homogeneous within analytical error. Table 2 compiles the analytical data for quijarroite (mean of 24 spot analyses; range, and standard deviation). Table 3 provides a selection of microprobe spot analysis on quijarroite, together with the elemental detection limits (d.l.).

The empirical formula of quijarroite (based on 25 *apfu*) is $(Cu_{05.84}Ag_{0.26})_{\Sigma = 6.10}(Hg_{1.06}Ni_{0.07}Co_{0.01})_{\Sigma = 1.14}$ $Pb_{2.27}Bi_{3.68}Se_{11.81}$. The ideal formula is $Cu_6HgPb_2Bi_4Se_{12}$, which requires (in wt %) Cu 13.72, Hg 7.22, Pb 14.91, Bi 30.06, Se 34.09, sum 100.00.

Table 2. Chemical data for quijarroite.

Element	Mean	Range	SD
Cu (wt %)	13.34	12.50–13.86	0.28
Ag	1.02	0.42–1.76	0.28
Hg	7.67	7.31–8.16	0.22
Pb	16.87	16.55–17.11	0.13
Co	0.03	0.00–0.11	0.04
Ni	0.15	0.00–0.45	0.15
Bi	27.65	27.37–28.05	0.19
Se	33.52	33.19–34.00	0.20
Total	100.24	99.64–100.65	0.30

Note: SD = 1σ standard deviation.

Table 3. Representative results of electron-microprobe spot analyses of quijarroite.

Element	d.l. (ppm)	1	2	3	4	5	6
Cu (wt %)	250	13.79	13.33	12.88	13.42	12.50	13.36
Ag	200	0.42	1.05	1.57	0.71	1.76	1.09
Hg	1100	7.56	7.96	7.40	7.31	7.75	8.16
Pb	400	16.86	16.90	16.76	16.93	16.76	16.79
Co	200	0	0.11	0.06	0	0	0
Ni	200	0.04	0.11	0.09	0.45	0.14	0
Bi	300	27.49	27.46	27.80	27.46	27.51	27.69
Se	800	33.86	33.39	33.19	33.36	33.60	33.49
Total		100.02	100.30	99.76	99.64	100.03	100.57
Cu (*apfu*)		6.02	5.84	5.69	5.88	5.51	5.85
Ag		0.11	0.27	0.41	0.18	0.46	0.28
Hg		1.04	1.10	1.04	1.02	1.08	1.13
Pb		2.26	2.27	2.27	2.28	2.27	2.25
Co			0.05	0.03			
Ni		0.02	0.05	0.04	0.21	0.07	
Bi		3.65	3.66	3.73	3.66	3.69	3.69
Se		11.90	11.76	11.79	11.77	11.92	11.80

Note: d.l. = detection limit.

5. X-ray Crystallography and Crystal Structure

Powder X-ray data (Cu $K\alpha$ radiation) were collected with an automated CCD-equipped Oxford Diffraction Xcalibur PX single-crystal diffractometer (Oxford Diffraction, Oxford, UK) using a Cu $K\alpha$ radiation (Gandolfi-type data collection). The measured and calculated (using the software *PowderCell* 2.3 [6]) powder diffraction patterns are given in Table 4. Unit-cell parameters refined from the collected data are as follows: a = 9.2376(8), b = 9.0176(7), c = 9.6198(8) Å, V = 801.34(8) Å^3, Z = 1.

For the X-ray single-crystal diffraction study, a small crystal fragment (0.03 × 0.035 × 0.05 mm^3) was handpicked from a fragment of the holotype specimen. The crystal was preliminarily examined with a Bruker-Enraf MACH3 single-crystal diffractometer using graphite-monochromatized Mo$K\alpha$ radiation. The data collection was then done with an Oxford Diffraction Xcalibur 3 diffractometer (Oxford Diffraction) (X-ray Mo$K\alpha$ radiation, λ = 0.71073 Å) fitted with a Sapphire 2 CCD detector (Oxford Diffraction) (see Table 5 for details). Intensity integration and standard Lorentz-polarization corrections were done with the *CrysAlis* RED [12] software package. The program ABSPACK of the *CrysAlis* RED package [12] was used for the absorption correction. The merging R for the ψ-scan data set decreased from 0.165 before absorption correction to 0.041 after this correction. Reflections conditions ($h0l$: $h + l = 2n$; $h00$: $h = 2n$; $00l$: $l = 2n$) were consistent with the space groups $Pmn2_1$, $P2_1nm$ and $Pmnm$, and the statistical tests on the distribution of $|E|$ values strongly indicated the absence of an inversion center ($|E^2 - 1| = 0.695$). The structure solution was then initiated in the standard setting

of space group *Pmn*2_1. The refined unit-cell parameters are *a* = 9.2413(8), *b* = 9.0206(7), *c* = 9.6219(8) Å, *V* = 802.1(1) Å^3, *Z* = 1.

Table 4. Measured and calculated X-ray powder diffraction data (*d* in Å) for quijarroite. The strongest diffraction lines are given in bold.

hkl	d_{meas}	I_{meas}	d_{calc}	I_{calc}
010	-	-	9.0206	47
101	6.65	20	6.6651	23
111	**5.36**	**55**	**5.3606**	**50**
002	4.82	20	4.8109	18
020	-	-	4.5103	12
012	-	-	4.2450	5
210	-	-	4.1125	6
120	-	-	4.0533	5
211	**3.785**	**60**	**3.7816**	**58**
202	**3.331**	**40**	**3.3325**	**45**
022	**3.291**	**90**	**3.2904**	**95**
220	3.228	25	3.2276	29
212	**3.125**	**100**	**3.1260**	**100**
122	-	-	3.0998	5
221	3.059	25	3.0600	30
030	-	-	3.0069	8
113	2.871	15	2.8723	16
031	-	-	2.8700	7
130	-	-	2.8593	5
222	-	-	2.6803	9
032	2.551	10	2.5498	12
213	-	-	2.5291	10
230	-	-	2.5202	11
014	-	-	2.3243	11
400	**2.312**	**50**	**2.3103**	**46**
040	2.256	10	2.2552	13
232	2.233	10	2.2325	15
033	-	-	2.1936	11
313	-	-	2.1572	6
024	-	-	2.1225	9
214	**2.078**	**35**	**2.0764**	**40**
241	-	-	1.9831	15
233	1.981	30	1.9816	29
332	-	-	1.9642	7
224	1.926	10	1.9287	12
422	1.888	30	1.8908	35
242	1.865	20	1.8677	22
050	-	-	1.8041	6
215	-	-	1.7430	9
234	-	-	1.7401	7
432	-	-	1.7121	6
414	-	-	1.6385	7
440	-	-	1.6138	8
433	-	-	1.5908	6
252	-	-	1.5865	6
424	-	-	1.5630	6
612	-	-	1.4479	7
614	-	-	1.2839	6
264	-	-	1.2290	6

Note: Calculated diffraction pattern obtained with the atom coordinates reported in Table 6 (only reflections with $I_{\text{rel}} \geq 5$ are listed).

Table 5. Crystal data and details of data collection and refinement for quijarroite.

Crystal Data	
space group	$Pmn2_1$
cell parameters	$a = 9.2413(8)$ (Å)
	$b = 9.0206(7)$ (Å)
	$c = 9.6219(8)$ (Å)
	$V = 802.1(1)$ (Å^3)
Z	1
crystal color	black
crystal shape	block
crystal size (mm^3)	$0.030 \times 0.035 \times 0.050$
Data Collection	
diffractometer	Oxford Diffraction Xcalibur III
radiation type	Mo$K\alpha$ ($\lambda = 0.71073$ Å)
monochromator	oriented graphite (002)
scan mode	φ/ω
temperature (K)	293
detector to sample distance (cm)	5
number of frames	702
rotation width per frame (°)	0.15
measuring time (s)	100
maximum covered 2θ (°)	60.02
range of *h*, *k*, *l*	$-13 \leq h \leq 13,\ -12 \leq k \leq 12,\ -13 \leq l \leq 13$
collected reflections	9312
R_{int} before absorption correction	0.0840
R_{int} after absorption correction	0.0235
Refinement	
refinement coefficient	F^2
No. of refl. in refinement	2195
No. of observed refl.	1523
No. of refined parameters	69
weighting scheme	$w = 1/[\sigma^2(I) + (0.044 \times I)^2]$
R [†] (obs)/R [†] (all)	0.0276/0.0281
w$R2$ [†] (obs)/w$R2$ [†] (all)	0.0242/0.0258
Flack parameter	$-0.002(9)$
diff. Fourier (e$^-$/Å^3)	$[-0.42, 0.76]$

Note: [†] $R = \Sigma||F_o| - |F_c||/|F_o|$. w$R2 = [\Sigma w(|F_o|^2 - |F_c|^2)^2/\Sigma w(|F_o|^4)]^{1/2}$.

The position of most of the atoms (i.e., Pb, Bi1, Bi2, Se2, Se3) was determined from the three-dimensional Patterson synthesis [13]. A least-squares refinement using these heavy-atom positions and isotropic temperature factors yielded an *R* factor of 10.4%. Three-dimensional difference Fourier synthesis yielded the position of the remaining metals and the two Se atoms. The full-matrix least-squares program SHELXL-97 [13] was used for the refinement of the structure. Site-scattering values were refined using scattering curves for neutral species [14] as follows: Hg vs. Cu, Pb vs. □, Bi vs. □ and Se vs. □, for the Cu, Pb, Bi and Se sites, respectively. Cu1 has a population of $Cu_{0.75}Hg_{0.25}$, whereas Cu2 is occupied at 75% (cf. Table 6). The Pb and Bi sites were found fully occupied. The Se sites were found to be fully occupied by Se. At the last stage, with anisotropic atomic displacement parameters for all atoms and no constraints, the residual value settled at $R = 0.027$ for 1523 independent observed reflections ($4\sigma(F_o)$ level) and 69 parameters and at $R = 0.028$ for all 2195 independent reflections. Inspection of the difference Fourier map revealed that the maximum positive and negative peaks were 0.42 and 0.76 e$^-$/Å^3, respectively. Wyckoff positions, site occupation factors, fractional atomic coordinates, and equivalent isotropic displacement parameters (Å^2) are given in Table 6. The main interatomic distances (Å) are reported in Table 7.

Table 6. Wyckoff positions, site occupation factors (s.o.f.), fractional atomic coordinates (*x*,*y*,*z*), and equivalent isotropic displacement parameters (U_{iso}, Å^2) for the selected quijarroite crystal.

Atom	Wyckoff	s.o.f.	x	y	z	U_{iso}
Cu1	4*b*	$Cu_{0.75(1)}Hg_{0.25}$	0.2311(3)	0.2658(4)	0.8228(4)	0.0381(11)
Pb	2*a*	$Pb_{1.00}$	$\frac{1}{2}$	0.4971(3)	0.1768(2)	0.0424(6)
Bi1	2*a*	$Bi_{1.00}$	$\frac{1}{2}$	0.0703(2)	0.0560(3)	0.0410(5)
Bi2	2*a*	$Bi_{1.00}$	0	0.5064(2)	0.1495(2)	0.0369(5)
Cu2	4*b*	$Cu_{0.75(2)}\square_{0.25}$	0.2437(6)	0.2757(9)	0.4230(11)	0.0430(2)
Se1	2*a*	$Se_{1.00}$	0	0.2400(6)	0.2794(6)	0.0342(11)
Se2	2*a*	$Se_{1.00}$	$\frac{1}{2}$	0.2319(6)	0.2990(6)	0.0340(11)
Se3	4*b*	$Se_{1.00}$	0.2373(4)	0.0861(5)	0.6428(5)	0.0362(8)
Se4	4*b*	$Se_{1.00}$	0.2685(4)	0.5532(5)	0.4925(5)	0.0374(8)

Table 7. Main interatomic distances (Å) for the studied quijarroite crystal.

Cu1-Se4 [i]	2.309(6)	Bi2-Se4 [vi]	2.673(4)
Cu1-Se3	2.373(6)	Bi2-Se4 [ii]	2.673(4)
Cu1-Pb [i]	3.333(4)	Bi2-Se1	2.708(6)
Pb-Se2	2.665(6)	Cu2-Se4	2.601(9)
Pb-Se4 [ii]	3.083(4)	Cu2-Se1	2.662(7)
Pb-Se4 [iii]	3.083(4)	Cu2-Se2	2.681(7)
Pb-Cu [iii]	3.333(4)	Cu2-Se3	2.72(1)
Bi1-Se3 [iv]	2.738(4)		
Bi1-Se3 [v]	2.738(4)		
Bi1-Se2	2.755(6)		

Note: Symmetry codes: (*i*) $-x + 1/2, -y + 1, z + 1/2$; (*ii*) $-x + 1/2, -y + 1, z - 1/2$; (*iii*) $x + 1/2, -y + 1, z - 1/2$; (*iv*) $-x + 1/2, -y, z - 1/2$; (*v*) $x + 1/2, -y, z - 1/2$; (*vi*) $x - 1/2, -y + 1, z - 1/2$.

The crystal structure of quijarroite (Figure 4) can be considered a galena derivative. It can be derived from that of bournonite [15]. The bournonite isotypic series recently encompassed three members: bournonite, $CuPbSbS_3$, seligmannite, $CuPbAsS_3$, and součekite, $CuPbBi(S,Se)_3$ [16]. The crystal structure of the latter is unknown but the similarity of the unit-cell parameters and the diffraction pattern with bournonite and seligmannite indicates that it is likely a member of this group. Overall, in their structure (orthorhombic, space group $Pn2_1m$), Pb forms 7,8-fold polyhedra, M^{3+} (M = Sb, As, Bi) forms trigonal pyramids, and Cu exhibits a tetrahedral coordination. All these polyhedra share corners and edges to form a three-dimensional network. CuS_4 tetrahedra share corners to form chains parallel to [001]. In quijarroite, Bi fully occupies the two 2*a* Wyckoff positions usually occupied by As and Sb in seligmannite and bournonite, respectively, Cu enters the same tetrahedral 4*b* position (with an occupancy of three-fourths of the site; refined site population: $Cu_{0.75}\square_{0.25}$), and Se fully replaces S at all the available anion positions. The most striking difference is what occurs at the Pb positions: In quijarroite only one of the two Pb positions of bournonite and seligmannite (2*b* Wyckoff position) is occupied by Pb, whereas the second is vacant and replaced by a general (4*b*) position occupied by Cu and Hg (refined site population: $Cu_{0.75}Hg_{0.25}$), showing an almost perfect linear coordination. A linear-coordinated mixed (Cu,Hg) site has been observed in some other phases, e.g., in the linearly coordinated Hg site of fettelite [17] or in rouxelite [18]. The linear-coordinated Cu/Hg atoms exhibit a mean bond distance of 2.342 Å, which leads to a bond valence sum (taking into account the parameters of Breese and O'Keeffe [19]) of 1.33 v.u. (vs. the ideal value of 1.25). The two Bi positions lead to 2.61 and 3.06 v.u. (for Bi1 and Bi2, respectively) and the Pb positions to a value of 1.74 v.u. The tetrahedral site exhibits a mean bond distance of 2.666 Å, which results in a bond valence sum of 0.73 v.u. (vs. the ideal value of 0.75, given the structural vacancy present at this site). If we compare the formula of quijarroite to that of the members of the bournonite group, we should write $[Cu_{0.75}\square_{0.25}][Cu_{0.75}Hg_{0.25}]Pb_{0.5}BiSe_3$, which leads to $Cu_{1.50}Hg_{0.25}Pb_{0.5}BiSe_3$ (with $Z = 4$), or $Cu_6HgPb_2Bi_4Se_{12}$ (with $Z = 1$). Quijarroite shows a strong enlargement of the unit-cell volume with respect to the members of the bournonite group (802.1(1) Å^3 vs. 538.8, 551.7 and 559.7 Å^3,

in seligmannite, bournonite and součekite, respectively). This increase is mainly due to the presence of Hg and Se replacing S.
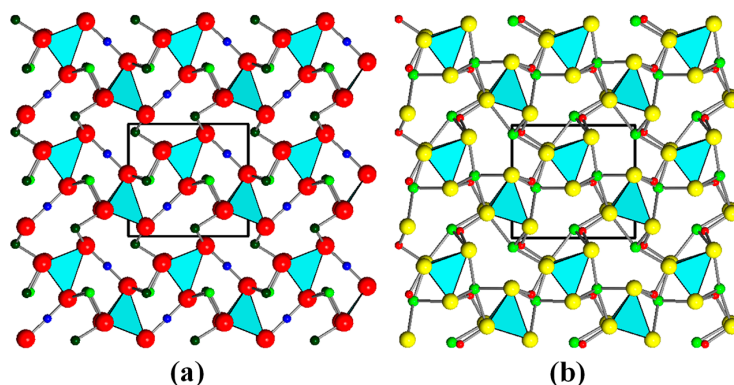

Figure 4. The crystal structure of quijarroite (**a**) compared to that of bournonite (**b**) [14], both drawn down [001]. In quijarroite, dark blue spheres indicate the linearly coordinated Cu/Hg atoms, whereas light blue tetrahedra refer to the partially occupied Cu position ($Cu_{0.75}\square_{0.25}$). Light, dark green and red spheres refer to Bi, Pb and Se, respectively. In bournonite, light blue tetrahedra refer to Cu, whereas green, red and yellow spheres refer to Pb, As and S, respectively.

6. Discussion

The new selenium mineral resembles phase "A" of Paar et al. (2012), for which the empirical formula $Cu_5Pb_2HgBi_3Se_{10}$ (normalized to 22 *apfu*) was proposed [2,4]. The identity of quijarroite with phase "A", for which no structural data were provided by Paar et al. (2012), is well displayed in a (Cu + Ag)−Hg−Bi diagram, where the mean compositions of both species overlap within analytical error (Figure 5).
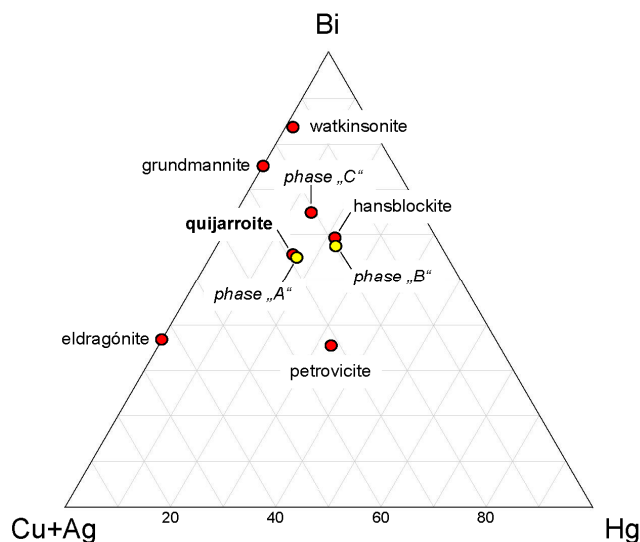
Figure 5. (Cu + Ag)−Hg−Bi (% *apfu*) ternary diagram showing the mean compositions of minerals of the Cu−Hg−Pb−Bi−Se system from El Dragón. Note the correspondence of quijarroite with phase "A" and hansblockite with phase "B" within analytical error. Data sources: [4,5], this paper and [2], for phases "A" and "B".

The new mineral is chemically close to a species termed "Bi-rich petrovicite" [20] from the Schlema-Alberoda U-Se-polymetallic deposit (Erzgebirge, Germany). Normalized to 12 Se, it would have the formula $Cu_{6.50}Hg_{0.96}Pb_{2.04}Bi_{3.72}Se_{12}$. This phase has also an orthorhombic cell, but different unit-cell parameters. If the structural data are correct, it might be a polymorph of quijarroite.

As to the physico-chemical environment of the formation of quijarroite, its commonly associated minerals provide little if any $p-T-x$ information. The stability relations of hansblockite and watkinsonite are largely unconstrained, and clausthalite has a broad stability field. Luckily, inferences could be made from the Cu selenides, with which quijarroite is occasionally intergrown. Thus, its association with umangite and klockmannite implies high selenium fugacities, above values defined by the umangite-klockmannite univariant reaction. At $T = 100\ °C$ and an elevated oxygen fugacity defined by the magnetite-hematite buffer, this relation would be consistent with a minimum log f_{Se_2} of roughly -14.5 [21]. The absence of end-member krut'aite and sulfides (chalcopyrite, pyrite) defines the maximum log f_{S_2} to roughly -19.

Author Contributions: Günter Grundmann collected the samples; Hans-Jürgen Förster and Günter Grundmann found the new mineral; Hans-Jürgen Förster conducted the electron-microprobe analyses; Luca Bindi performed the X-ray structural investigations; Chris J. Stanley and Günter Grundmann determined the optical and physical properties; Hans-Jürgen Förster wrote the paper.

Conflicts of Interest: The authors declare no conflict of interest.

References

1. Grundmann, G.; Lehrberger, G.; Schnorrer-Köhler, G. The El Dragón mine, Potosí, Bolivia. *Mineral. Rec.* **1990**, *21*, 133–146.

2. Paar, W.H.; Cooper, M.A.; Moëlo, Y.; Stanley, C.J.; Putz, H.; Topa, D.; Roberts, A.C.; Stirling, J.; Raith, J.G.; Rowe, R. Eldragónite, $Cu_6BiSe_4(Se)_2$, a new mineral species from the El Dragón mine, Potosí, Bolivia, and its crystal structure. *Can. Mineral.* **2012**, *50*, 281–294. [CrossRef]

3. Mills, S.J.; Kampf, A.R.; Christy, A.G.; Housley, R.M.; Thorne, B.; Chen, Y.S.; Steele, I.M. Favreauite, a new selenite mineral from the El Dragón mine, Bolivia. *Eur. J. Mineral.* **2014**, *26*, 771–781. [CrossRef]

4. Förster, H.-J.; Bindi, L.; Stanley, C.J. Grundmannite, $CuBiSe_2$, the Se-analogue of emplectite: A new mineral from the El Dragón mine, Potosí, Bolivia. *Eur. J. Mineral.* **2016**, *28*, 467–477. [CrossRef]

5. Förster, H.-J.; Bindi, L.; Stanley, C.J.; Grundmann, G. Hansblockite, $(Cu,Hg)(Bi,Pb)Se_2$, the monoclinic polymorph of grundmannite, a new mineral from the Se mineralization at El Dragón (Bolivia). *Mineral. Mag.* **2016**. [CrossRef]

6. Kampf, A.R.; Mills, S.J.; Nash, B.P.; Thorne, B.; Favreau, G. Alfredopetrovicite: A new selenite mineral from the El Dragón mine, Bolivia. *Eur. J. Mineral.* **2016**, *28*, 479–484. [CrossRef]

7. Bindi, L.; Förster, H.-J.; Grundmann, G.; Keutsch, F.N.; Stanley, C.J. Petříčekite, $CuSe_2$, a new member of the marcasite group from the Předbořice deposit, Central Bohemia Region, Czech Republic. *Minerals* **2016**, *6*, 33. [CrossRef]

8. Cunningham, C.A.; Aparicio, H.N.; Murillo, F.S.; Jiménez, N.C.; Lizeca, J.-L.B.; McKee, E.H.; Ericksen, G.E.; Tavera, F.V. *The Relationship between the Porco, Bolivia, Ag−Zn−Pb−Sn Deposit, and the Porco Caldera*; US Geological Survey Open-File Report, Series Number 94-238; U.S. Geological Survey: Reston, VA, USA, 1993.

9. El Dragón Mine, Antonio Quijarro Province, Potosí Department, Bolivia. Available online: http://www.mindat.org/loc-353.html (accessed on 17 November 2016).

10. Grundmann, G.; Förster, H.-J. Origin of the El Dragón selenium mineralization, Quijarro Province, Potosí, Bolivia. *Minerals*, in preparation.

11. Armstrong, J.T. CITZAF: A package of correction programs for the quantitative electron microbeam X-ray-analysis of thick polished materials, thin films, and particles. *Microbeam Anal.* **1995**, *4*, 177–200.

12. Oxford Diffraction. *CrysAlis RED (Version 1.171.31.2) and ABSPACK in CrysAlis RED*; Oxford Diffraction Ltd.: Oxfordshire, UK, 2006.

13. Sheldrick, G.M. A short history of SHELX. *Acta Crystallogr. Sect. A* **2008**, *64*, 112–122. [CrossRef] [PubMed]

14. Ibers, J.A.; Hamilton, W.C. (Eds.) *International Tables for X-Ray Crystallography*; Kynock: Dordrecht, The Netherlands, 1974; Volume IV, p. 366.

15. Edenharter, A.; Nowacki, W.; Takéuchi, Y. Verfeinerung der Kristallstruktur von Bournonit $[(SbS_3)_2 \mid Cu^{IV}_2Pb^{VII}Pb^{VIII}]$ und von Seligmannit $[(AsS_3)_2 \mid Cu^{IV}_2Pb^{VII}Pb^{VIII}]$. *Z. Krist.* **1970**, *131*, 397–417. [CrossRef]

16. Moëlo, Y.; Makovicky, E.; Mozgova, N.N.; Jambor, J.L.; Cook, N.; Pring, A.; Paar, W.H.; Nickel, E.H.; Graeser, S.; Karup-Møller, S.; et al. Sulfosalt systematics: A review. Report of the sulfosalt sub-committee of the IMA Commission on Ore Mineralogy. *Eur. J. Mineral.* **2008**, *20*, 7–46. [CrossRef]

17. Bindi, L.; Keutsch, F.N.; Francis, C.A.; Menchetti, S. Fettelite, $[Ag_6As_2S_7][Ag_{10}HgAs_2S_8]$ from Chañarcillo, Chile: Crystal structure, pseudosymmetry, twinning, and revised chemical formula. *Am. Mineral.* **2009**, *94*, 609–615. [CrossRef]

18. Orlandi, P.; Meerschaut, A.; Moëlo, Y.; Palvadeau, P.; Léone, P. Lead-antimony sulfosalts from Tuscany (Italy). VIII. Rouxelite, $Cu_2HgPb_{22}Sb_{28}S_{64}(O,S)_2$, a new sulfosalt from Buca della Vena mine, Apuan Alps: Definition and crystal structure. *Can. Mineral.* **2005**, *43*, 919–933. [CrossRef]

19. Breese, N.E.; O'Keeffe, M. Bond-valence parameters for solids. *Acta Crystallogr.* **1991**, *B47*, 192–197. [CrossRef]

20. Dymkov, Y.M.; Ryzhov, B.I.; Zav'yalov, Y.N.; Tsvetkova, M.V.; Shcherbachev, D.K. Bismuth variety of petrovicite from dolomitic veins of the Erzgebirge. *Trans. Dokl. USSR Acad. Sci. Earth Sci. Sect.* **1990**, *306*, 1451–1455.

21. Simon, G.; Kesler, S.E.; Essene, E.J. Phase relations among selenides, sulphides, tellurides, and oxides: II. Applications to selenide-bearing ore deposits. *Econ. Geol.* **1997**, *92*, 468–484. [CrossRef]